European Heart Journal – Cardiovascular Imaging (2013) **14**, 1049–1060
doi:10.1093/ehjci/jet049

# Contrast echocardiography for assessing left ventricular vortex strength in heart failure: a prospective cohort study

**Haruhiko Abe[1,2], Giuseppe Caracciolo[1,2], Arash Kheradvar[3], Gianni Pedrizzetti[2,4], Bijoy K. Khandheria[5], Jagat Narula[2], and Partho P. Sengupta[2]***

[1]Division of Cardiovascular Diseases, Mayo Clinic, Scottsdale, AZ, USA; [2]Zena and Michael A. Wiener Cardiovascular Institute, Mount Sinai School of Medicine, One Gustave L. Levy Place, PO Box 1030, New York, NY 10029, USA; [3]Department of Biomedical Engineering, University of California, Irvine, CA, USA; [4]Dipartimento Ingegneria e Architettura, University of Trieste, Italy; and [5]Aurora Sinai/Aurora St Luke's Medical Centers, University of Wisconsin School of Medicine and Public Health, Milwaukee, WI, USA

*Received 28 December 2012; accepted after revision 12 March 2013; online publish-ahead-of-print 14 April 2013*

**Aims** This study investigated the incremental role of echocardiographic-contrast particle image velocimetry (Echo-PIV) in patients with heart failure (HF) for measuring changes in left ventricular (LV) vortex strength (VS) during phases of a cardiac cycle.

**Methods and results** Echo-PIV was performed in 42 patients, including 23 HF patients and 19 controls. VS was measured as a fluid-dynamic parameter that integrates blood flow rotation over a given area and correlated with non-invasively derived indices of LV mechanical performance. In comparison with early and late diastole, the VS was higher during isovolumic contraction (IC) for control and HF patients with the preserved ejection fraction ($P = 0.002$ and $P = 0.01$, respectively), but not for HF patients with the reduced ejection fraction ($P = 0.41$). On multivariable regression analysis, the VS during IC ($VS_{IC}$) was independently related to late-diastolic VS and LV longitudinal strain ($R^2 = 0.63$, $P < 0.001$ and $P = 0.003$, respectively). Patients in whom diastolic VS was augmented during IC showed a higher LV stroke volume ($P = 0.01$), stroke work ($P = 0.02$), and mechanical efficiency ($P = 0.008$). Over a median follow-up period of 2.9 years, eight (34%) HF patients were hospitalized for decompensated HF. In comparison with the rest, these eight patients showed markedly reduced longitudinal strain ($P = 0.002$), and lower change in VS ($P = 0.004$).

**Conclusion** Our preliminary data suggest that the persistence of vortex from late diastole into IC is a haemodynamic measure of coupling between diastole and systole. The change in VS is correlated with LV mechanical performance and shows association with adverse clinical outcomes seen in HF patients.

**Keywords** Particle image velocimetry • Vortex • Left ventricle • Mechanical efficiency • Heart failure

## Introduction

Several numerical models, *in vitro* experiments, and imaging studies have shown that the transmitral blood flow during early-diastolic filling results in the formation of a left ventricular (LV) intracavitary vortex.[1–8] The LV vortex has been suggested to minimize kinetic energy dissipation and reduces the total energy required for eventual ejection.[1–8] Preliminary observations have further suggested that LV remodelling results in attenuation of the blood flow kinetic energy.[9] Given the complexity and the number of assumptions involved in experimental studies and relative dearth of data in humans, confirmation of proposed flow dynamics with the direct measurement of the blood flow sequence in clinical settings is crucial.

Kilner *et al.*[10] suggested that diastolic vortices are preserved by asymmetry of the flow paths that facilitate continued redirection of the blood flow towards the LV outflow for optimal ejection. Furthermore, the vortex formed in diastole persists into the period of isovolumic contraction (IC), which follows the mitral valve closure and is characterized by a rapid rise in LV pressure

* Corresponding author: The Mount Sinai Medical Center, One Gustave L. Levy Place, PO Box 1030, New York, New York 10029. Tel: +1 212 659 9121; Fax: +1 212 849 2674. Email: partho.sengupta@mountsinai.org

before opening of the aortic valve.[11] An organized LV intracavitary blood flow into IC may enhance coupling between diastole and systole, optimizing LV performance; however, the relationship of the LV flow to wall mechanics is a topic that has not been directly validated in clinical settings.

Echocardiographic-contrast particle image velocimetry (Echo-PIV) allows flow quantification;[12] its concept has been approve for vascular measurements and validated in accurate *in vitro* settings.[12–14] The feasibility of Echo-PIV for visualizing the LV flow has been recently validated[15,16] and potential applications have been verified in experimental[11] and clinical settings.[16] For the present investigation, we hypothesized that the strength of vortex persisting from diastolic filling into IC is a haemodynamic marker, that is, associated with LV mechanical performance. The present investigation, therefore, explored the spatial and temporal characteristics of the two-dimensional (2D) blood flow in relation to LV mechanical activity in compensated heart failure (HF) patients attending outpatient clinic (ACC/AHA Stage C or D HF).[17] Vortex strength (VS) was quantified as the total rotation rate of the flow in a bounded region. Asymptomatic patients with risk factors who were found to have normal LV structure and function on screening echocardiograms (ACC/AHA Stage A)[17] were used as a non-HF control group.

# Methods

We identified 47 consecutive subjects including 27 consecutive patients with Stage C or D compensated HF and 20 asymptomatic patients with risk factors who underwent an outpatient echocardiogram between July 2008 and July 2010 with a single provider (P.S.). The subjects were subsequently consented for an additional contrast echocardiogram. Exclusion criteria included decompensated HF, LV aneurysm, inotropic support at the time of evaluation, atrial fibrillation, hypertrophic or restrictive cardiomyopathy, pericardial diseases, valve disease (valvular stenosis or more than mild valvular regurgitation), primary pulmonary hypertension, congenital heart disease, acute coronary event or coronary artery bypass graft surgery (within 3 months), pregnancy, and patient refusal/inability to sign the informed consent form. Of the 47 patients, 5 were excluded because of suboptimal 2D or contrast echocardiographic image quality. Of the remaining 42 patients, 23 belonged to Stage C or D compensated HF with 10 patients having preserved ejection fraction (HFPEF) and 13 patients having the reduced ejection fraction (HFREF; $<$50%). Demographic features, risk factors, New York Heart Association class, and treatment are shown in *Table 1*. The institutional review board approved the study and all patients provided written informed consent.

## Standard B-mode and Doppler echocardiography

Cine loops from three standard apical views (four-chamber, two-chamber, and apical long-axis) and short-axis views at the mitral valve, papillary and apical levels were recorded using greyscale harmonic imaging (Vivid 7, GE Medical Systems, Horten, Norway), following the guidelines recommended by the American Society of Echocardiography.[18] End-diastolic and end-systolic volumes were used to calculate the ejection fraction by Simpson's biplane method from the apical four- and two-chamber views. Pulsed-wave Doppler echocardiography was performed to obtain early and late-diastolic transmitral flow velocities. Pulsed-wave tissue Doppler velocities were measured at the septal and lateral mitral annulus in the four-chamber view and were averaged for obtaining mean early-diastolic mitral annulus velocity and the ratio of early-diastolic transmitral flow velocity to early-diastolic mitral annulus velocity. Diastolic dysfunction and its severity was described as per the published recommendations.[19] We also calculated LV sphericity index,[20] LV stroke work,[21] and LV mechanical efficiency (ratio of stroke work/myocardial oxygen consumption, simplified as the amount of blood pumped by a single heart beat in 1 s.[22–25]), as per previously determined definitions.

## Speckle-tracking strain echocardiography

LV subendocardial longitudinal and circumferential strain and radial strain from full thickness of the myocardium were measured (50–80 frames/s) using the 2D Cardiac Performance Analysis© software (TomTec Imaging Systems, Munich, Germany), an extended version of a previously validated software (*syngo*® Velocity Vector Imaging™, Siemens Medical Solutions USA, Inc., Malvern, PA, USA).[26] Net LV twist was calculated as the net difference between LV peak rotation angles obtained from basal (CW, clockwise) and apical (CCW, counterclockwise) short-axis planes. Dyssynchrony was measured as the standard deviation of the time to minimum (for longitudinal and circumferential) or to maximum (for radial) strain obtained from 16 LV segments.

## Contrast echocardiography

Two-dimensional contrast echocardiography was performed with a perfluoropropane gas-filled, lipid-stabilized microbubble (Definity®, Lantheus Medical Imaging, Inc., North Billerica, MA, USA; 0.1–0.2 mL infused intravenously as bolus injection). Two-dimensional images of the intraventricular flow were obtained from the apical long-axis view at a mechanical index of 0.1–0.4. The width and depth of the ultrasound scan area (*Figure 1*) and the spatial temporal settings were optimized to achieve the highest possible frame rates (204 $\pm$ 39 frames/s).

Images were acquired when the bubble density and motion were optimal and best visually appreciable. On the one hand, the density of bubble had to be sufficient to appreciate their individual motion, on the other, saturation had to be avoided to make bubbles distinguishable. To verify this, we first obtained anatomical M-mode images from the 2D contrast scans along the central scanning axis as described previously (*Figure 2*).[11] This acquisition ensures that the same bubbles remain in the scan plane for finite period of time resulting into the formation of streaks in the dark blood pool. The presence of these streaks ensures that the bubble density is optimal for creating speckle patterns that can be tracked in the ultrasonic scan plane. Nevertheless, it was previously demonstrated theoretically[27] that the bubble density has only a weak influence on the results of image analysis for blood motion.

## Echocardiographic particle image velocimetry

Echo-PIV uses pairs of sequential digital images for calculating the direction and magnitude of the fluid flow.[12,14,16] For this, contrast images with particles were exported into files as a stack of images during a cardiac cycle and were analysed frame by frame with a PIV software (time-resolved analysis, INSIGHT™ 3G TSI, Inc., Shoreview, MN, USA[11]) to obtain the velocity vector field (*Figure 1*). The interrogation window of 32 $\times$ 64 pixels with 50% overlap was used for analysis. Maximal particle displacement was $<$16 pixels in *x*-axis direction and $<$32 pixels in *y*-axis direction during the first interrogation and adjusted until optimal Echo-PIV tracking was achieved. The reliability of the evaluated velocities that may be affected by either local

**Table 1. Baseline characteristics of study subjects**

| | Non-HF control ($n = 19$) | Heart failure | | *P*-value |
|---|---|---|---|---|
| | | HFPEF ($n = 10$) | HFREF ($n = 13$) | |
| Age (years) | 61 ± 10 | 65 ± 12 | 75 ± 7*,*** | 0.001 |
| Female gender (%) | 8 (42) | 3 (30) | 1 (7) | 0.10 |
| Body surface area ($m^2$) | 1.88 ± 0.28 | 1.87 ± 0.20 | 1.98 ± 0.19 | 0.37 |
| Systolic blood pressure (mmHg) | 132 ± 17 | 129 ± 19 | 135 ± 22 | 0.80 |
| Diastolic blood pressure (mmHg) | 77 ± 10 | 70 ± 15 | 73 ± 10 | 0.21 |
| Heart rate (beats/min) | 67 ± 11 | 72 ± 19 | 72 ± 13 | 0.71 |
| PR (ms) | 156 ± 17 | 132 ± 30 | 142 ± 38 | 0.05 |
| QRS (ms) | 88 ± 10 | 117 ± 29** | 167 ± 40*,*** | <0.001 |
| QRS >120 ms (%) | 1 (5) | 4 (40) | 11 (84) | <0.001 |
| Left bundle branch block (%) | 1 (5) | 0 (0) | 3 (23) | 0.15 |
| NYHA class | — | 1.3 ± 0.6 | 2.1 ± 0.9 | 0.02 |
| Risk factors (%) | | | | |
| Diabetes | 2 (10) | 3 (30) | 5 (38) | 0.16 |
| Hypertension | 10 (52) | 4 (40) | 9 (69) | 0.36 |
| Hyperlipidaemia | 8 (42) | 4 (40) | 11 (84) | 0.03 |
| Coronary artery disease | 2 (10) | 1 (10) | 8 (61) | 0.002 |
| Renal failure(Cr >1.2) | 0 (0) | 6 (60) | 5 (38) | 0.37 |
| Medications (%) | | | | |
| ACEI or ARB | 1 (5) | 3 (30) | 10 (76) | <0.001 |
| Beta blocker | 4 (21) | 7 (70) | 11 (84) | <0.001 |
| Calcium-channel blocker | 2 (10) | 3 (30) | 1 (7) | 0.25 |
| Digoxin | — | — | 4 (30) | — |
| Diuretics | 2 (10) | 8 (80) | 8 (61) | <0.001 |

EF, ejection fraction; HFPEF, HF with preserved EF; HFREF, HF with the reduced ejection fraction; NYHA, New York Heart Association; ACEI, angiotensin-converting enzyme inhibitor; ARB, angiotensin receptor blocker.
*$P < 0.05$ non-HF control vs. HFREF.
**$P < 0.05$ non-HF control vs. HFPEF.
***$P < 0.05$ HFPEF vs. HFREF.

absence or contrary excessive saturation of contrast agent is automatically monitored by the software by excluding vectors with small cross-correlation coefficient. To find subpixel displacement, we used a three-point, two-direction, Gaussian peak fitting in one dimension Illustrative figures and movies were prepared using the dedicated software (Hyperflow, Amid.net, Sulmona, Italy).

Once the velocity field was obtained, the spatial distribution of *vorticity* was computed, at every frame, using Tecplot (Tecplot, Inc., Bellevue, Washington, DC, USA). Vorticity, which corresponds to the local angular velocity of a fluid particle, represents the key quantity in fluid dynamics as it permits the delineation and quantification of vortices and shear layers. Mathematically, it is computed by taking the curl of velocity vector. Vorticity ($i, j, t$) was calculated by numerical derivatives.

$$\text{Vorticity} = 1000 \times \left\{ \frac{Vy(i+1,j) - Vy(i-1,j)}{x(i+1,j) - x(i-1,j)} - \frac{Vx(i,j+1) - Vx(i,j-1)}{y(i,j+1) - y(i,j-1)} \right\}$$
$$= 1000 \times \left( \frac{dVy}{dx} - \frac{dVx}{dy} \right).$$

Units are as follows: $x$ (mm), $y$ (mm), $Vx$ (m/s), and $Vy$ (m/s).

Vorticity is a useful quantity to describe the underlying structure of a moving fluid. A region with compact vorticity represents a region with circular streamlines and constitutes a vortex; a region with elongated vorticity distribution exhibits a difference of velocity between the two sides and, thus, constitutes a shear layer, which serves as a boundary layer in vicinity of the wall. A brief introduction of the role vorticity for the cardiac flow has been recently reviewed[28]; and a more in-depth discussion on the same topic can be found elsewhere.[29]

In integral terms, vorticity defines the amount of circulatory (swirling) fluid dynamics. To evaluate such a feature of the motion, vorticity distribution was plotted in the form of a histogram based on the percentage of the map area vs. the vorticity values $\omega$ ($s^{-1}$) throughout the entire flow map (*Figure 3*). Based on conventions, CCW and CW vorticity are represented in red and blue, respectively, on the contour map.

Following the procedure outlined in *Figure 3*, we further characterized the amount of CW and CCW swirl by the circulation, that is, computed by taking the product of the corresponding mean vorticity and the area occupied by such vorticity within the area enclosed by the scanned image boundary. VS refers to the total amount of swirl (or circulation), and was calculated by summing up the value of the both the CW and the CCW values of the circulation. Early and late diastole and IC periods were delineated as previously described[11] and average VS was calculated during each of these three periods.

$VS_{IC}$ was considered augmented if the magnitude was greater than the VS attained during early or late diastole ($VS_E$ or $VS_A$). We also calculated the absolute change in VS from early diastole to IC and expressed it as a fractional change in VS from early diastole to IC ($[VS_{IC} - VS_E]/VS_{IC}$).

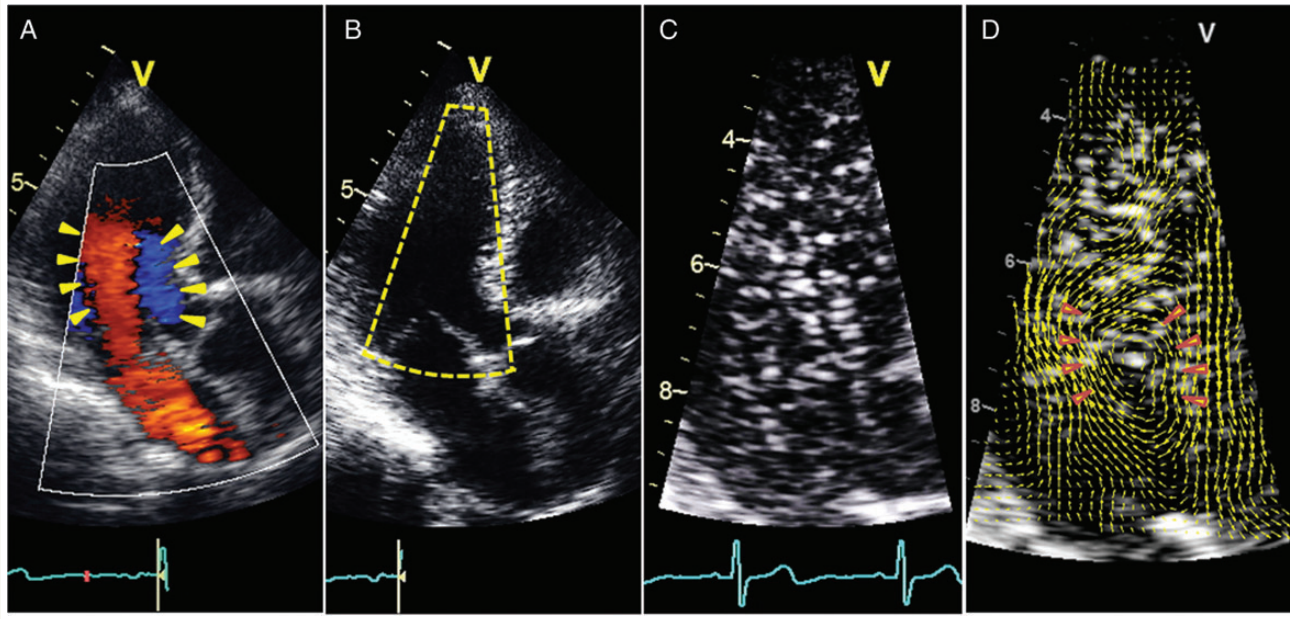


**Figure 1.** Echocardiographic-contrast particle imaging velocimetry. (*A*) Colour Doppler imaging showing the bidirectional flow during early diastole. (*B*) Delineation of the region of interest in the submitral and LV outflow region. (*C*) High-temporal resolution contrast echocardiography is performed for the region of interest. (*D*) Contrast particle imaging velocimetry shows the flow field with velocity vectors. Note the presence of a CW vortex (arrows).

## Follow-up

Observed survival was assessed through a search of medical records and the Social Security Death Index on 1 November 2011. Rehospitalization for decompensated HF and all-cause mortality was recorded for each of the 23 HF patients from the date of echocardiography through November 2011, resulting in a median length of follow-up of 2.9 years. The following clinical events were reported as endpoints: cardiac death, hospitalization due to cardiac decompensation, or necessity for heart transplantation. The first event that occurred was used for the analysis.

## Statistical analysis

Statistical analysis was performed with commercially available software (MedCalc 11.2, MedCalc Software, Mariakerke, Belgium). All continuous data were reported as means ± standard deviation, and categorical data as percentages. The Kruskal–Wallis test was used for non-parametric comparisons among independent non-HF control and HF groups and the Friedman test was used for non-parametric comparisons of repeated measurements of VS among cardiac cycle phases. The Mann–Whitney *U*-test was used for non-parametric comparisons of unpaired measurements between non-HF control and/or HF groups and the Wilcoxon rank-sum test was used for non-parametric comparisons of paired measurements of VS between cardiac cycle phases. The $\chi^2$ test was used for comparisons of categorical variables. Univariate and multivariate linear regression analysis was performed to determine correlates of $VS_{IC}$. Statistical significance was defined as a two-tailed *P*-value $<0.05$. Intra-observer and inter-observer variability for the measurement of VS were calculated as means ± standard deviations of percentage ratios between absolute differences and means of the two independently measured variables in 10 randomly selected patients. Inter-observer agreement and intra-observer consistency were assessed with the Bland–Altman analysis.[30]

# Results

## Clinical characteristics

Differences in baseline clinical and echocardiographic characteristics for HF patients and non-HF controls are shown in *Tables 1* and *2*, respectively. HFREF patients were older ($P = 0.001$) with a higher prevalence of coronary artery disease ($P = 0.002$) and prolongation of QRS interval on surface electrocardiogram ($P < 0.001$). On echocardiography, HFREF patients showed significantly larger left atrial volume ($P = 0.004$), greater LV remodelling with the increased LV dimensions and sphericity index ($P < 0.001$ for each), and significantly increased ratio of the early-diastolic flow to mitral annular lengthening velocity ($P = 0.001$; *Table 2*). In comparison with non-HF controls and HFPEF, global LV strains in longitudinal, circumferential and radial directions, and net twist were significantly reduced in HFREF patients ($P < 0.05$ for each). Similarly, in comparison with non-HF controls and HFPEF, HFREF patients showed the presence of significant dyssynchrony in the longitudinal direction ($P = 0.01$).

## LV fluid dynamics

For non-HF control, both $VS_E$ and $VS_A$ were similar in magnitude; however, the magnitude of $VS_{IC}$ was significantly higher than $VS_E$ and $VS_A$ ($P = 0.01$ vs. and 0.002, respectively). Although $VS_E$ in patients with HFPEF was lower than in non-HF controls ($P = 0.09$) and not different from $VS_A$, the magnitude of $VS_{IC}$

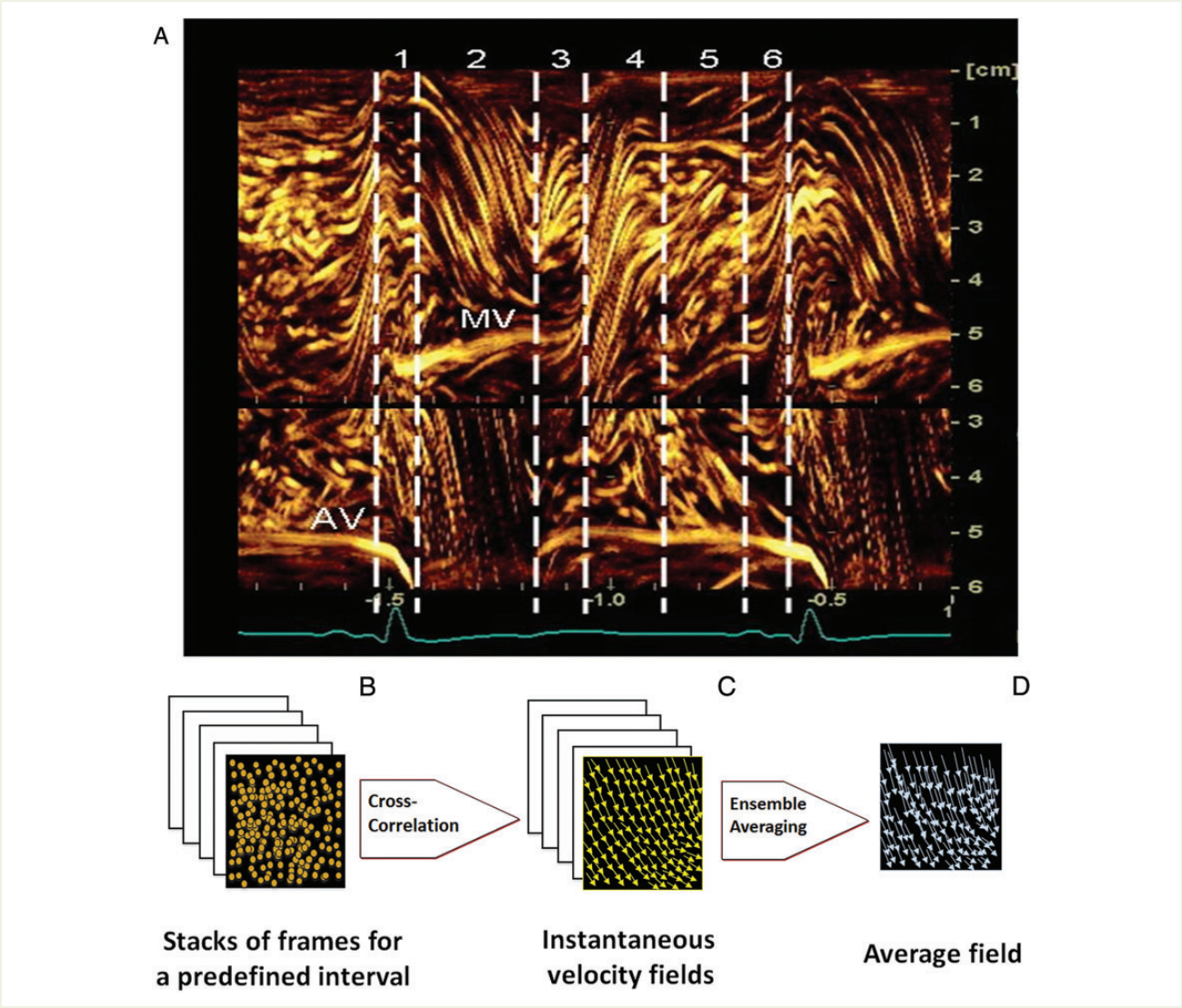


**Figure 2.** Assessment of LV intracavitary flow, contrast density, and motion. (*A*) An anatomical M-mode through the LV cavity during contrast infusion. The axial movement of contrast bubbles produces bright streaks, which suggest optimum contrast density and temporal resolution for tracking. The phases of cardiac cycle are then determined using the movement of the MV and the AV. Phases: 1, pre-ejection; 2, ejection; 3, isovolumic relaxation; 4, early diastole; 5, diastasis; and 6, late diastole. (*B*) Series of phase locked image frames are obtained during time intervals through the cardiac cycle as defined above. (*C*) Sequential pairs of these frames are cross-correlated for obtaining the velocity vectors. (*D*) Ensemble average of the sequential vector fields obtained for each time interval defines the dominant flow features in the flow field for that specific time interval.

was augmented and higher than $VS_A$ ($P = 0.01$). In contrast, for patients with HFREF, $VS_E$ was not significantly different than in non-HF controls, however, $VS_{IC}$ failed to augment to a value higher than $VS_E$ or $VS_A$ (*Table 2* and *Figures 4* and *5*).

To understand the factors that contribute to $VS_{IC}$, we examined the univariate relationships between $VS_{IC}$ and LV muscle and fluid mechanics variables (*Table 3*). On multivariable regression analysis, the magnitude of $VS_{IC}$ was independently related to $VS_E$ and LV longitudinal strain ($R^2 = 0.63$, $P < 0.001$). Similarly, the presence of dyssynchrony in the longitudinal strain was associated with $VS_{IC}$ in HF patients ($r = -0.54$, $P = 0.04$). Supplementary data online, *Movies S1* and *S2* show a non-HF control subject with VS, that is, higher in IC, whereas Supplementary data online, *Movies S3* and *S4* illustrate an example of attenuated $VS_{IC}$ in a patient with HFREF. The presence of greater $VS_{IC}$ than the highest VS recorded during the diastolic phases was associated with a higher LV stroke volume (odds ratio: 1.09; confidence interval: 1.02–1.17; $P = 0.011$), stroke work (odds ratio: 1.03; confidence interval: 1.00–1.06; $P = 0.02$), and LV mechanical efficiency (odds ratio: 1.05; confidence interval: 1.01–1.10; $P = 0.008$). LV mechanical efficiency was related to longitudinal strain ($r = -0.38$, $P = 0.05$), radial strain ($r = 0.45$, $P = 0.005$), net LV twist ($r = 0.34$, $P = 0.02$), and VS change ($r = 0.38$, $P = 0.01$).

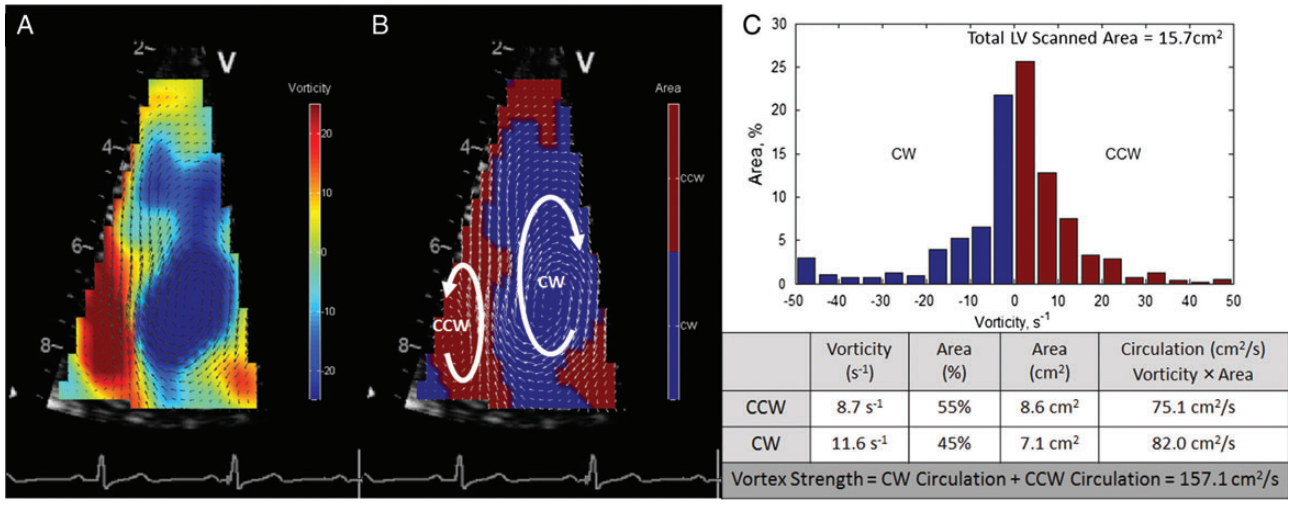


| | Vorticity ($s^{-1}$) | Area (%) | Area ($cm^2$) | Circulation ($cm^2/s$) Vorticity × Area |
|---|---|---|---|---|
| CCW | 8.7 $s^{-1}$ | 55% | 8.6 $cm^2$ | 75.1 $cm^2/s$ |
| CW | 11.6 $s^{-1}$ | 45% | 7.1 $cm^2$ | 82.0 $cm^2/s$ |
| Vortex Strength = CW Circulation + CCW Circulation = 157.1 $cm^2/s$ | | | | |

**Figure 3.** Calculation of circulation as a measure of VS. (*A*) Ensemble averaged vorticity distribution during early diastole. (*B*) Flow areas are separated into regions with CCW (red colour) and CW (blue colour) vorticity. (*C*) A histogram of CCW (positive vorticity) and CW (negative vorticity) is weighted by the percentage of area that takes such a value. Thus, the mean value of the positive and the negative vorticity is evaluated and the percentage of the corresponding areas is evaluated by summing up the histogram bins. The VS is computed by adding the circulation in CW and CCW directions (circulation is obtained by multiplying the mean vorticity with the corresponding areas).

## Clinical follow-up and adverse events

Follow-up data were analysed in HF patients over a median follow-up period of 2.9 years. Of 23 patients, eight (34%) were hospitalized for decompensated HF, five (21%) patients died, and 1 patient underwent cardiac transplantation. Patients who reached an endpoint of death or hospitalization for HF ($n = 8$) showed a lower ejection fraction ($P = 0.08$) than remaining of the HF patients; however, had similar LA volumes and diastolic dysfunction. Patients with endpoints showed significantly lower longitudinal strain ($P = 0.002$), circumferential strain ($P = 0.04$), radial strain ($P = 0.02$), and lower change in VS ($P = 0.004$). The difference in VS change between the two groups persisted even after adjusting for the differences in LV EF ($P = 0.03$) (*Table 4*).

## Inter-observer and intra-observer variability

The inter-observer and intra-observer variability for VS measurements were 7.7 ± 7.9 and 7.3 ± 7.8%, respectively. Bland–Altman analysis was used to assess inter-observer agreement and intra-observer consistency. Mean values, their differences, and the intraclass correlation coefficients are shown in Supplementary data online, *Table S1*. VS had good reproducibility with intraclass correlation coefficients ≥0.95 for most evaluations.

# Discussion

This is the first prospective study that has (i) tested the phasic changes in the strength of intraventricular flow rotation (VS) in HF patients, using a fluid-dynamic variable computed through a high-temporal resolution Echo-PIV, which permits flow characterization during the phases of the cardiac cycle including the brief isovolumic phases, (ii) correlated the change in VS with non-invasively derived markers of LV systolic and diastolic performance including LV deformation and twist mechanics, and (iii) provided preliminary data regarding the change in VS from early diastole to IC in patients with HF with normal or reduced ejection fraction with further follow-up over a median period of 2.9 years for characterizing the potential prognostic value of change in VS.

## VS during phases of cardiac cycle

A vortex develops in the form of a shear layer adjacent to the tissue (boundary layer). When the shear layer separates from the wall, fluid tends to curl into a vortex.[29] Previous investigations have studied the transmitral vortex formation using numerical or physical models or through flow visualization techniques such as cardiac magnetic resonance,[2,10,31–33] colour Doppler and contrast echocardiography.[11,16,34] The LV vortex characteristics in previous studies, however, have been primarily related to the diastolic filling phases of the cardiac cycle.[2–5,31,35] In an experimental model, we described the persistence of the LV vortex in early systole during the IC period; however, the relation between vortex during IC and LV mechanical activity was not previously assessed.[11] In a subsequent investigation, we also reported a close coupling of LV late-diastolic and IC mechanical activity and its utility in predicting peak oxygen consumption during exercise.[36] The present investigation further demonstrates the mechanical continuum of late-diastolic and IC phases of the cardiac cycle. A circulating blood flow during late diastole is smoothly continued into the phase of IC; where it becomes the eventual outcome of the diastolic vortex formation process that can relate with the LV mechanical activity

**Table 2. Echocardiographic variables of study subjects**

| | Control ($n = 19$) | Heart failure | | *P*-value |
|---|---|---|---|---|
| | | HFPEF ($n = 10$) | HFREF ($n = 13$) | |
| Standard echocardiography | | | | |
| LV septum (mm) | 9 ± 1 | 11 ± 2 | 10 ± 2 | 0.11 |
| LV posterior wall (mm) | 9 ± 1 | 11 ± 2 | 10 ± 2 | 0.35 |
| LV end-diastolic dimension (mm) | 45 ± 6 | 44 ± 4 | 62 ± 7[*,***] | <0.001 |
| LV end-systolic dimension (mm) | 30 ± 4 | 29 ± 4 | 52 ± 9[*,***] | <0.001 |
| LVEF (%) | 63 ± 5 | 61 ± 7 | 28 ± 10[*,***] | <0.001 |
| LV EDV (mL) | 114 ± 40 | 113 ± 33 | 202 ± 79[*,***] | <0.001 |
| LV ESV (mL) | 41 ± 22 | 43 ± 17 | 146 ± 76[*,***] | <0.001 |
| LVEF (%) | 63 ± 5 | 61 ± 7 | 28 ± 10[*,***] | <0.001 |
| Indexed LA volume (mL/m$^2$) | 32 ± 9 | 43 ± 12[**] | 48 ± 21[*] | 0.004 |
| E velocity (m/s) | 0.74 ± 0.12 | 0.80 ± 0.29 | 0.80 ± 0.26 | 0.98 |
| *E/A* ratio | 1.1 ± 0.3 | 1.5 ± 0.6 | 1.7 ± 1.5 | 0.13 |
| *E/e′* mean | 9.5 ± 3.1 | 13.3 ± 7.2[**] | 22.5 ± 12.4[*] | 0.001 |
| Normal diastolic function (%) | 14 (63) | — | — | — |
| Diastolic dysfunction (%) | 5 (26) | 10 (100) | 13 (100) | <0.001 |
| Grade I (%) | 5 (26) | 2 (20) | 4 (31) | |
| Grade II (%) | — | 7 (70) | 4 (31) | |
| Grade III (%) | — | 1 (10) | 5 (38) | |
| RVSP (mmHg) | 28 ± 5 | 39 ± 11[**] | 42 ± 15[*] | 0.007 |
| LV sphericity index | 0.54 ± 0.05 | 0.54 ± 0.05 | 0.65 ± 0.09[*,***] | <0.001 |
| LV stroke volume (mL) | 73 ± 19 | 70 ± 22 | 56 ± 14 | 0.08 |
| LV stroke work (g) | 119 ± 42 | 110 ± 43 | 90 ± 26 | 0.30 |
| LV mechanical efficiency (mL/s) | 69 ± 28 | 63 ± 26 | 49 ± 19 | 0.16 |
| Strain, twist, and dyssynchrony | | | | |
| Ls (%) | −18.3 ± 4.4 | −15.2 ± 5.8 | −9.8 ± 5.2[*,***] | <0.001 |
| Cs (%) | −23.8 ± 4.6 | −22.6 ± 7.4 | −11.2 ± 6.1[*,***] | <0.001 |
| Rs (%) | 24.6 ± 9.6 | 19.7 ± 11.6 | 8.7 ± 5.2[*,***] | <0.001 |
| Net twist (degree) | 10.9 ± 5.6 | 11.7 ± 9.2 | 5.5 ± 3.6[*] | 0.02 |
| SD of time to Ls (ms) | 50 ± 21 | 49 ± 23 | 81 ± 27[*] | 0.01 |
| SD of time to Cs (ms) | 83 ± 31 | 69 ± 38 | 82 ± 40 | 0.61 |
| SD of time to Rs (ms) | 126 ± 47 | 116 ± 44 | 165 ± 63 | 0.17 |
| Echocardiographic PIV | | | | |
| $VS_E$ (cm$^2$/s) | 184 ± 57 | 143 ± 67 | 182 ± 67 | 0.19 |
| $VS_A$ (cm$^2$/s) | 184 ± 67 | 143 ± 47 | 207 ± 118 | 0.15 |
| $VS_{IC}$ (cm$^2$/s) | 231 ± 85[****,*****] | 195 ± 103[****,*****] | 203 ± 88 | 0.24 |
| VS change | 0.12 ± 0.33 | 0.21 ± 0.33 | 0.06 ± 0.24 | 0.37 |

LV, left ventricular; EF, ejection fraction; EDV, end-diastolic volume; ESV, end-systolic volume; LA, left atrium; E, early diastole; A, late diastole; *E/e′*, ratio of early-diastolic transmitral flow velocity to early-diastolic tissue velocity; RVSP, right ventricular systolic pressure; Ls, longitudinal strain; Cs, circumferential strain; Rs, radial strain; PIV, particle imaging velocimetry; $VS_{IC}$, vortex strength during isovolumic contraction; $VS_E$, vortex strength in early diastole; $VS_A$, vortex strength in late diastole; SD, standard deviation.
[*]$P < 0.05$ control vs. HFREF.
[**]$P < 0.05$ control vs. HFPEF.
[***]$P < 0.05$ HFPEF vs. HFREF.
[****]$P < 0.05$ $VS_{IC}$ vs. $VS_E$.
[*****]$P < 0.05$ $VS_{IC}$ vs. $VS_A$.

in systole. This suggests a potential role of IC vortex in optimizing diastolic-to-systolic mechanical coupling.

## VS in HF

During the IC period, shortening of early activated regions of LV is accompanied with stretching of the late activated regions.[37,38] This reshaping deformation suggests interactions between the blood flow sequence and the LV mechanical activity developing in early systole.[39] Indeed, structural and functional remodelling of the LV results in an unfavourable mechanoenergetic profile (i.e. diminished mechanical efficiency)[40] and this change in mechanical efficiency may be related to the attenuation of the kinetic energy

of the diastolic LV flow.[9] Furthermore, a reduction in VS, during the IC period, may alter contractility of activated myocytes due to variations in preload that influence the steepness of the Frank–Starling relationship.[39] These novel insights, which link LV geometry, muscle, and fluid mechanics, raise several interesting hypotheses that require further verification.

## Methodological considerations

The Echo-PIV technique has been previously validated in the laminar flow[41] and in the carotid bifurcation[14] with good agreement seen with optical particle imaging velocimetry for *in vitro* models of the pulsatile flow.[15,16]. However, the feasibility of using Echo-PIV in routine hospital settings for 2D contrast echocardiography for LV cavity opacification has not been sufficiently clarified. A recent experimental study assessed Echo-PIV accuracy against optical PIV for LV flow visualization and revealed a tendency to underestimate the higher velocity when traditional clinical settings were used (frame rate $< 100$ Hz).[12,16] We attempted to circumvent some of these limitations by using lower contrast particle density for optimal PIV tracking and using a much higher temporal resolution (frame rate: 129–252 Hz). Moreover, previous works that used Echo-PIV in clinics,[34] or in a validation study,[16] employed different parameters because the frame rates were insufficient for quantitatively evaluating velocities values and parameters were designed merely as a statistical measure of the overall flow pattern. The technique employed here presents, instead, a sufficient acquisition frame rate that allowed evaluating actual fluid-dynamics quantities that were further related with LV muscle mechanics.

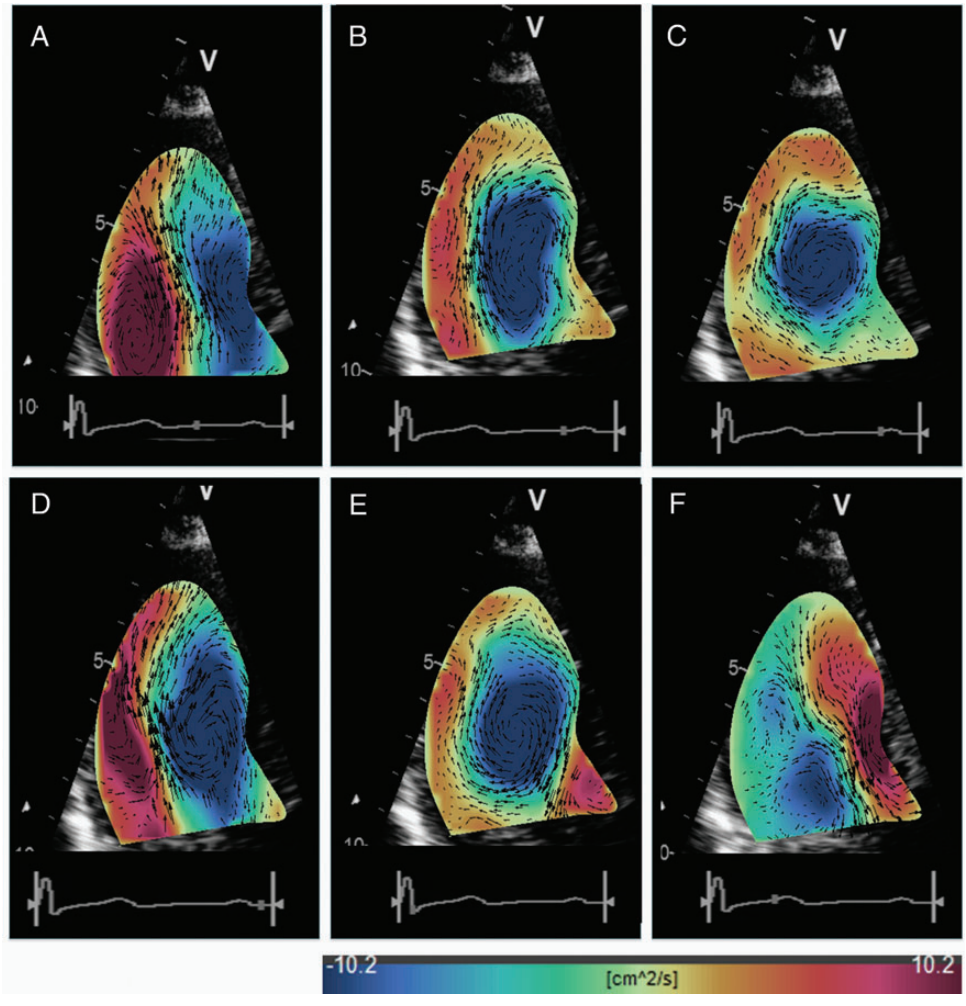


**Figure 4.** The LV flow sequence during phases of cardiac cycles in a non-HF control subject. LV intracavitary planar vorticity maps of a non-HF control subject (EF 61%) during phases of cardiac cycle are shown in (*A*–*F*). Note that the presence of initial CW (blue) and CCW (red) vortex during early-diastolic filling (*A*). The counterclockiwise flow (red) becomes weaker (*B*) resulting into predominantly CW (blue) vortex during the phase of diastasis (*C*). The atrial flow in late diastole is characterized by an increase in the strength of the CW vortex (*D*), which persists further during IC (*E*). Ejection is characterized by accelerating flow towards the LV outflow surrounded by CW and CCW shear layers (*F*). Movies corresponding to Figure 3 can be viewed as Supplementary data online, *Movies S1* and *S2*.

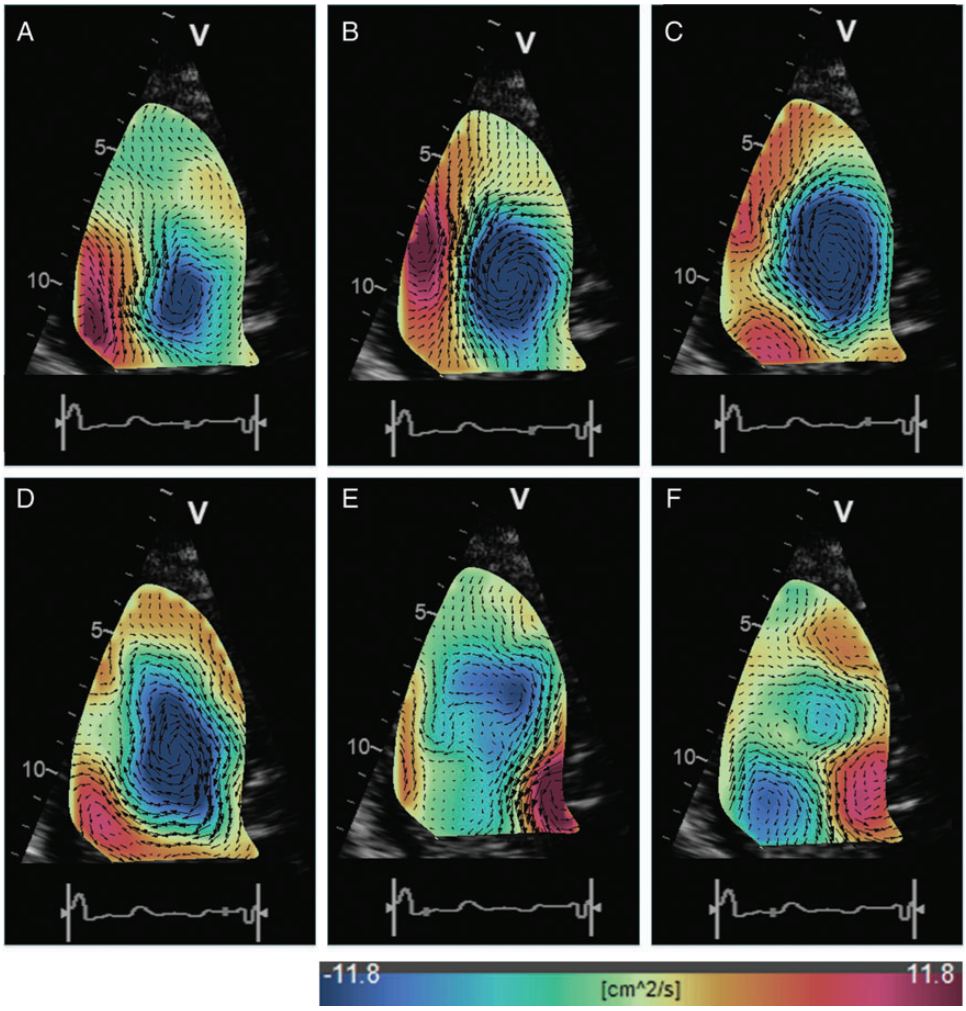


**Figure 5.** The LV flow sequence in HFREF. LV intracavitary planar vorticity maps of a Stage C HFREF patient (EF 34%) during phases of the cardiac cycle are shown in (*A*–*F*). The cardiac cycle (*A*–*F*) is the same as outlined in Figure 3. Note that the CW vortex is attenuated during IC (*E*). Movies corresponding to Figure 4 can be viewed as Supplementary data online, *Movies S3* and *S4*.

## Clinical significance

Clinical investigators have recently debated the binary view to HF using the terms systolic and diastolic HF.[42] These data would support the recent suggestions that properties of failing hearts should be considered at different hierarchical scales of performance for understanding the levels of mechanical inefficiencies rather than merely relegating to binary divisions of systolic and diastolic dysfunction.[42] Such integrative analysis of levels of energetic inefficiencies in a failing heart may provide a logical approach to characterizing multidimensional complex interactions between biomarkers in HF syndromes.[43] Although attempts at energetic efficiency of the blood flow were recently measured using the MRI-based assessment of blood flow fields,[44] Echo-PIV is an extension of the LV opacification technique and can be performed in minutes from LV contrast opacification, which is frequently used in HF patients.[45] Another advantage of Echo-PIV is the high-temporal resolution, which permits tracking the blood flow sequence during the transient isovolumic phases of the cardiac cycle. Therefore, the development of echocardiographic techniques for flow visualization has potential for providing a practical technique for characterizing the degree of flow inefficiency in HF patients in clinical practice.

## Study limitations

We used apical long-axis views for focusing on the dominant flow structures in the inflow and the outflow regions of the LV. Use of a full 3D structure of flow with incorporation of boundaries would be necessary for more complete assessment of the LV flow structure. The relationships between VS and the ventricle's mechanical performance shown in this investigation also need cautious interpretation. First, the VS alone may not account for other aspects, like the vortex position and its shape with respect to the LV chamber, which may play a role in the flow arrangement and influence LV performance. Furthermore, the formula used for calculating LV

**Table 3. Univariate and multivariate linear regression analysis for correlates of VS during IC**

| | Univariate regression | | Multivariate regression | | | | |
|---|---|---|---|---|---|---|---|
| | Correlation | *P*-value | B | SE | *t*-value | *P*-value | $R^2$ |
| $VS_A$ ($cm^2/s$) | 0.70 | <0.001 | 0.75 | 0.10 | 7.31 | <0.001 | 0.63 |
| $VS_E$ ($cm^2/s$) | 0.57 | <0.001 | | | | | |
| Ls (%) | −0.34 | 0.02 | −4.44 | 1.41 | −3.14 | 0.003 | |
| Cs (%) | −0.25 | 0.10 | | | | | |
| Rs (%) | 0.28 | 0.06 | | | | | |
| Net twist (degree) | 0.30 | 0.05 | | | | | |

$VS_A$, vortex strength during late diastole; $VS_E$, vortex strength during early diastole; Ls, longitudinal strain; Cs, circumferential strain; Rs, radial strain.

**Table 4. Clinical and echocardiographic features of HF patients with and without adverse clinical events during follow-up**

| | Heart failure | | *P*-value |
|---|---|---|---|
| | Without events (*n* = 15) | With events (*n* = 8) | |
| Age (years) | 71 ± 11 | 71 ± 9 | 0.97 |
| Female gender (%) | 4 (30) | — | 0.30 |
| HFPEF (*n*) (%) | 7 (46) | 3 (37) | 0.98 |
| Standard echocardiography | | | |
| LV septum (mm) | 11 ± 2 | 10 ± 2 | 0.60 |
| LV end-diastolic dimension (mm) | 52 ± 7 | 58 ± 15 | 0.27 |
| LV end-systolic dimension (mm) | 39 ± 10 | 50 ± 16 | 0.12 |
| LVEF (%) | 47 ± 16 | 34 ± 21 | 0.08 |
| Indexed LA volume ($mL/m^2$) | 46 ± 21 | 46 ± 8 | 0.49 |
| *E*/*A* ratio | 1.3 ± 0.5 | 2.2 ± 1.7 | 0.14 |
| *E*/*e*′ mean | 14.7 ± 6.5 | 24.7 ± 14.0 | 0.10 |
| RVSP (mmHg) | 40 ± 10 | 44 ± 18 | 0.75 |
| LV sphericity index | 0.66 ± 0.15 | 0.72 ± 0.15 | 0.39 |
| LV stroke volume (mL) | 65 ± 18 | 59 ± 21 | 0.63 |
| LV stroke work (g) | 101 ± 31 | 83 ± 29 | 0.21 |
| LV mechanical efficiency (mL/s) | 61 ± 23 | 46 ± 22 | 0.26 |
| Global strains and twist | | | |
| Ls (%) | −14.6 ± 4.6 | −7.6 ± 5.9 | 0.002 |
| Cs (%) | −19.0 ± 8.2 | −10.9 ± 7.4 | 0.04 |
| Rs (%) | 15.9 ± 9.7 | 9.0 ± 9.6 | 0.02 |
| Net twist (degree) | 9.5 ± 8.1 | 5.7 ± 4.3 | 0.20 |
| Echocardiographic PIV | | | |
| $VS_E$ ($cm^2/s$) | 143 ± 67 | 182 ± 67 | 0.29 |
| $VS_A$ ($cm^2/s$) | 192 ± 117 | 155 ± 40 | 0.54 |
| $VS_{IC}$ ($cm^2/s$) | 219 ± 108 | 162 ± 32 | 0.42 |
| VS change | 0.24 ± 0.24 | −0.08 ± 0.24 | 0.004 |

Abbreviations are similar as in *Table 2*.

mechanical efficiency was simplified as the ratio between stroke volume and heart rate. Although this has been shown to provide useful information,[22–25] this theoretical approach differs from previous equations where energy consumption is determined by coronary sinus catheterization to measure real-time myocardial oxygen consumption. Finally, although the difference in VS was associated with adverse cardiac events, the number of events was small and precluded a detailed survival analysis.

# Conclusions

The present study establishes the sequence in which LV vortices formed during diastolic filling phases are sustained into IC for the optimal onset of ejection. Our data suggest that the persistence of VS from late diastole into IC is a marker of the fluid-continuum of the cardiac cycle and helps coupling diastole to systole without any intervening periods of haemodynamic stasis. The change in VS is correlated with LV mechanical performance and may have prognostic value for HF patients.

# Supplementary data

Supplementary data are available at *European Heart Journal – Cardiovascular Imaging* online.

## Funding

This study was supported by an intramural fund (CR-5) from Mayo Clinic, Scottsdale, AZ, USA.

**Conflict of interest**: none declared.

## References

1. Baccani B, Domenichini F, Pedrizzetti G, Tonti G. Fluid dynamics of the left ventricular filling in dilated cardiomyopathy. *J Biomech* 2002;**35**:665–71.
2. Gharib M, Rambod E, Kheradvar A, Sahn DJ, Dabiri JO. Optimal vortex formation as an index of cardiac health. *Proc Natl Acad Sci USA* 2006;**103**:6305–8.
3. Kheradvar A, Gharib M. Influence of ventricular pressure drop on mitral annulus dynamics through the process of vortex ring formation. *Ann Biomed Eng* 2007;**35**:2050–64.
4. Kheradvar A, Gharib M. On mitral valve dynamics and its connection to early diastolic flow. *Ann Biomed Eng* 2009;**37**:1–13.
5. Pedrizzetti G, Domenichini F. Nature optimizes the swirling flow in the human left ventricle. *Phys Rev Lett* 2005;**95**:108101.
6. Saber NR, Wood NB, Gosman AD, Merrifield RD, Yang GZ, Charrier CL *et al.* Progress towards patient-specific computational flow modeling of the left heart via combination of magnetic resonance imaging with computational fluid dynamics. *Ann Biomed Eng* 2003;**31**:42–52.
7. Subramanian A, Mu H, Kadambi JR, Wernet MP, Brendzel AM, Harasaki H. Particle image velocimetry investigation of intravalvular flow fields of a bileaflet mechanical heart valve in a pulsatile flow. *J Heart Valve Dis* 2000;**9**:721–31.
8. Taylor TW, Yamaguchi T. Flow patterns in three-dimensional left ventricular systolic and diastolic flows determined from computational fluid dynamics. *Biorheology* 1995;**32**:61–71.
9. Carlhall CJ, Bolger A. Passing strange: flow in the failing ventricle. *Circ Heart Fail* 2010;**3**:326–31.
10. Kilner PJ, Yang GZ, Wilkes AJ, Mohiaddin RH, Firmin DN, Yacoub MH. Asymmetric redirection of flow through the heart. *Nature* 2000;**404**:759–61.
11. Sengupta PP, Khandheria BK, Korinek J, Jahangir A, Yoshifuku S, Milosevic I *et al.* Left ventricular isovolumic flow sequence during sinus and paced rhythms: new insights from use of high-resolution Doppler and ultrasonic digital particle imaging velocimetry. *J Am Coll Cardiol* 2007;**49**:899–908.
12. Crapper M, Bruce T, Gouble C. Flow field visualization of sediment-lsaden flow using ultrasonic imaging. *Dyn Atmos Oceans* 2000;**31**:233–45.
13. Kim H, Hertzberg J, Shandas R. Development and validation of echo PIV. *Exp Fluids* 2004;**36**:455–62.
14. Zhang F, Lanning C, Mazzaro L, Barker AJ, Gates PE, Strain WD *et al.* In vitro and preliminary in vivo validation of echo particle image velocimetry in carotid vascular imaging. *Ultrasound Med Biol* 2011;**37**:450–64.
15. Westerdale J, Belohlavek M, McMahon EM, Jiamsripong P, Heys JJ, Milano M. Flow velocity vector fields by ultrasound particle imaging velocimetry: in vitro comparison with optical flow velocimetry. *J Ultrasound Med* 2011;**30**:187–95.
16. Kheradvar A, Houle H, Pedrizzetti G, Tonti G, Belcik T, Ashraf M *et al.* Echocardiographic particle image velocimetry: a novel technique for quantification of left ventricular blood vorticity pattern. *J Am Soc Echocardiogr* 2010;**23**:86–94.
17. Hunt SA, Abraham WT, Chin MH. 2009 Focused Update Incorporated into the ACC/AHA 2005 Guidelines for the Diagnosis and Management of Heart Failure in Adults: a Report of the American College of Cardiology Foundation/American Heart Association Task Force on Practice Guidelines Developed in Collaboration with the International Society for Heart and Lung Transplantation (vol 53, pg e1, 2009). *J Am Coll Cardiol* 2009;**54**:2464–4.
18. Lang RM, Bierig M, Devereux RB, Flachskampf FA, Foster E, Pellikka PA *et al.* Recommendations for chamber quantification: a report from the American Society of Echocardiography's Guidelines and Standards Committee and the Chamber Quantification Writing Group, developed in conjunction with the European Association of Echocardiography, a branch of the European Society of Cardiology. *J Am Soc Echocardiogr* 2005;**18**:1440–63.
19. Nagueh SF, Appleton CP, Gillebert TC, Marino PN, Oh JK, Smiseth OA *et al.* Recommendations for the evaluation of left ventricular diastolic function by echocardiography. *Eur J Echocardiogr* 2009;**10**:165–93.
20. Yiu SF, Enriquez-Sarano M, Tribouilloy C, Seward JB, Tajik AJ. Determinants of the degree of functional mitral regurgitation in patients with systolic left ventricular dysfunction: a quantitative clinical study. *Circulation* 2000;**102**:1400–6.
21. de Simone G, Devereux RB, Ganau A, Hahn RT, Saba PS, Mureddu GF *et al.* Estimation of left ventricular chamber and stroke volume by limited M-mode echocardiography and validation by two-dimensional and Doppler echocardiography. *Am J Cardiol* 1996;**78**:801–7.
22. de Simone G, Chinali M, Galderisi M, Benincasa M, Girfoglio D, Botta I *et al.* Myocardial mechano-energetic efficiency in hypertensive adults. *J Hypertens* 2009;**27**:650–5.
23. Schramm W. The units of measurement of the ventricular stroke work: a review study. *J Clin Monit Comput* 2010;**24**:213–7.
24. Cioffi G, Russo TE, Selmi A, Stefenelli C, Furlanello F. Analysis of left ventricular systolic function by midwall mechanics in patients with obstructive sleep apnoea. *Eur J Echocardiogr* 2011;**12**:61–8.
25. Kozakova M, Malshi E, Morizzo C, Pedri S, Santini F, Biolo G *et al.* Impact of prolonged cardiac unloading on left ventricular mass and longitudinal myocardial performance: an experimental bed rest study in humans. *J Hypertens* 2011;**29**:137–43.
26. Pirat B, Khoury DS, Hartley CJ, Tiller L, Rao L, Schulz DG *et al.* A novel feature-tracking echocardiographic method for the quantitation of regional myocardial function: validation in an animal model of ischemia-reperfusion. *J Am Coll Cardiol* 2008;**51**:651–9.
27. Gao H, Claus P, Amzulescu MS, Stankovic I, D'Hooge J, Voigt JU. How to optimize intracardiac blood flow tracking by echocardiographic particle image velocimetry? Exploring the influence of data acquisition using computer-generated data sets. *Eur Heart J Cardiovasc Imaging* 2012;**13**:490–9.
28. Sengupta PP, Pedrizzetti G, Kilner PJ, Kheradvar A, Ebbers T, Tonti G *et al.* Emerging trends in CV flow visualization. *JACC Cardiovasc Imaging* 2012;**5**:305–16.
29. Kheradvar A, Pedrizzetti G. *Vortex Formation in the Cardiovascular System*. London: Springer-Verlag, 2012.
30. Bland JM, Altman DG. Statistical methods for assessing agreement between two methods of clinical measurement. *Lancet* 1986;**1**:307–10.
31. Kim WY, Walker PG, Pedersen EM, Poulsen JK, Oyre S, Houlind K *et al.* Left ventricular blood flow patterns in normal subjects: a quantitative analysis by three-dimensional magnetic resonance velocity mapping. *J Am Coll Cardiol* 1995;**26**:224–38.
32. Bolger AF, Heiberg E, Karlsson M, Wigstrom L, Engvall J, Sigfridsson A *et al.* Transit of blood flow through the human left ventricle mapped by cardiovascular magnetic resonance. *J Cardiovasc Magn Reson* 2007;**9**:741–7.
33. Walker PG, Cranney GB, Grimes RY, Delatore J, Rectenwald J, Pohost GM *et al.* Three-dimensional reconstruction of the flow in a human left heart by using magnetic resonance phase velocity encoding. *Ann Biomed Eng* 1996;**24**:139–47.
34. Hong GR, Pedrizzetti G, Tonti G, Li P, Wei Z, Kim JK *et al.* Characterization and quantification of vortex flow in the human left ventricle by contrast echocardiography using vector particle image velocimetry. *JACC Cardiovasc Imaging* 2008;**1**:705–17.
35. Ishizu T, Seo Y, Ishimitsu T, Obara K, Moriyama N, Kawano S *et al.* The wake of a large vortex is associated with intraventricular filling delay in impaired left ventricles with a pseudonormalized transmitral flow pattern. *Echocardiography* 2006;**23**:369–75.
36. Cho EJ, Caracciolo G, Khandheria BK, Steidley DE, Scott R, Abhayaratna WP *et al.* Tissue Doppler image-derived measurements during isovolumic contraction predict exercise capacity in patients with reduced left ventricular ejection fraction. *JACC Cardiovasc Imaging* 2010;**3**:1–9.
37. Rankin JS, McHale PA, Arentzen CE, Ling D, Greenfield JC Jr, Anderson RW. The three-dimensional dynamic geometry of the left ventricle in the conscious dog. *Circ Res* 1976;**39**:304–13.
38. Sengupta PP, Korinek J, Belohlavek M, Narula J, Vannan MA, Jahangir A *et al.* Left ventricular structure and function: basic science for cardiac imaging. *J Am Coll Cardiol* 2006;**48**:1988–2001.
39. Sengupta PP. Exploring left ventricular isovolumic shortening and stretch mechanics: 'The heart has its reasons...'. *JACC Cardiovasc Imaging* 2009;**2**:212–5.

40. Knaapen P, Germans T, Knuuti J, Paulus WJ, Dijkmans PA, Allaart CP *et al.* Myocardial energetics and efficiency: current status of the noninvasive approach. *Circulation* 2007;**115**:918–27.
41. Kim HB, Hertzberg J, Lanning C, Shandas R. Noninvasive measurement of steady and pulsating velocity profiles and shear rates in arteries using echo PIV: in vitro validation studies. *Ann Biomed Eng* 2004;**32**:1067–76.
42. De Keulenaer GW, Brutsaert DL. Systolic and diastolic heart failure are overlapping phenotypes within the heart failure spectrum. *Circulation* 2011;**123**:1996–2004; discussion 2005.
43. Azuaje FJ, Dewey FE, Brutsaert DL, Devaux Y, Ashley EA, Wagner DR. Systems-based approaches to cardiovascular biomarker discovery. *Circ Cardiovasc Genet* 2012;**5**:360–7.
44. Eriksson J, Dyverfeldt P, Engvall J, Bolger AF, Ebbers T, Carlhall CJ. Quantification of presystolic blood flow organization and energetics in the human left ventricle. *Am J Physiol Heart Circ Physiol* 2011;**300**:H2135–41.
45. Kurt M, Shaikh KA, Peterson L, Kurrelmeyer KM, Shah G, Nagueh SF *et al.* Impact of contrast echocardiography on evaluation of ventricular function and clinical management in a large prospective cohort. *J Am Coll Cardiol* 2009;**53**:802–10.

**IMAGE FOCUS**

doi:10.1093/ehjci/jet095
Online publish-ahead-of-print 18 May 2013

# Is it really fat? Ask a T1-map

**Vanessa M. Ferreira*, Cameron J. Holloway, Stefan K. Piechnik, Theodoros D. Karamitsos, and Stefan Neubauer**

Department of Cardiovascular Medicine, University of Oxford, John Radcliffe Hospital, Oxford, UK

* Corresponding author. Tel: +44 1865221873; fax: +44 1865740449; Email: vanessa.ferreira@cardiov.ox.ac.uk

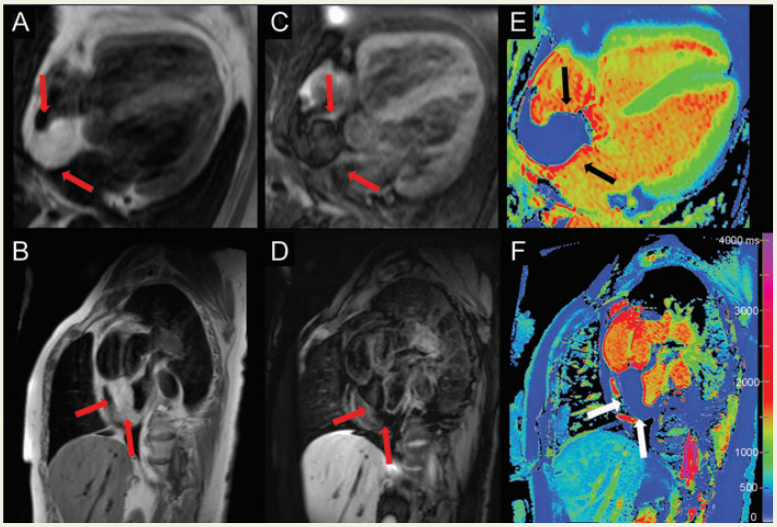


A 67-year-old woman initially presented with dyspnoea. Echocardiography demonstrated an inter-atrial mass. Cardiovascular magnetic resonance (CMR) showed a well-marginated mass (35 mm × 45 mm) in the inter-atrial septum (IAS) sparing the fossa ovalis, extending to the posterior right atrial wall. The mass had high signal intensity on T1-weighted images (*Panels A* and *B*, arrows) consistent with fat, which attenuated on fat-suppression imaging (*Panels C* and *D*, arrows). Native T1-maps (*Panels E* and *F*, arrows) showed homogenous and significantly lower T1 values (230–350 ms) compared with the normal myocardium (green) and blood (yellow/red), but similar to subcutaneous and epicardial fat (blue). The mass had no late gadolinium enhancement and was stable in the size compared with 1-year prior. Findings were consistent with lipomatous hypertrophy of the IAS.

This is a first demonstration of using native T1-mapping for immediate visual and quantitative tissue characterization of an intracardiac mass to help confirm its fat content. T1-maps provide pixel-wise estimates of the T1 relaxation times of the underlying tissue, and each tissue type exhibits a characteristic normal range of T1 values. This allows the visual differentiation of tissues using colour scales as shown. Lipomatous hypertrophy of the IAS is an unencapsulated proliferation of adipose tissue ≥20 mm within the atrial septum that is in continuity with epicardial fat. It is associated with older age, increased fat elsewhere in the body, atrial arrhythmias and in some cases, obstruction of the superior vena cava. The correct differentiation of this benign cardiac mass from other atrial tumours using multi-parametric tissue characterization techniques on CMR can prevent unnecessary invasive interventions.

## Funding

Funding to pay the Open Access publication charges for this article was provided by the Division of Cardiovascular Medicine, Radcliffe Department of Medicine, University of Oxford.